

Understanding glass-like Vogel-Fulcher-Tammann equilibration times: microcanonical effective temperatures in quenched 3D martensites

N. Shankaraiah¹, K.P.N. Murthy² and S.R. Shenoy¹

¹Tata Institute of Fundamental Research-Hyderabad, Hyderabad, Telangana 500046, India.

²Dept of Physics, Central University of Rajasthan, Bandar Sindri, Rajasthan 305817, India

(Dated: September 12, 2022)

We do Monte Carlo simulations of four 3D structural transitions, with vector-spin models of their martensitic strain domains under quenches to T , to test a generic post-quench Partial Equilibration Scenario (PES) of Ritort. We indeed confirm that energy-lowering passages between fixed-energy shells induce a signature PES distribution of an exponential tail in heat releases, scaled in an effective search temperature. A linear vanishing of this $T_{eff}(T) \sim T_d - T$ at a temperature T_d where PES passage-searches freeze, explains the Vogel-Fulcher like divergence of equilibration times $e^{1/T_{eff}(T)} \sim e^{1/(T_d - T)}$, extracted from incubation-time delays of simulations and martensitic alloys.

Glassy freezing or structural arrest of a rapidly cooled liquid or colloidal system¹⁻⁵ that pre-empts crystallisation, has been investigated for more than a century. Supercooled liquid models can yield heterogeneous domains of competing crystal structures^{3,5}. Equilibration time divergences at a glassy freezing temperature T_G , have been fitted to Vogel-Fulcher-Tammann (VFT) $\sim e^{1/T - T_G}$, or other forms^{2,4}. It is natural to study generic equilibration scenarios⁶⁻⁹ in specific structural-domain systems that have long relaxation times^{1-5,10-16}.

After a sudden quench, a system on a free energy landscape, has competing pathways to the new global minimum, delayed by free energy barriers $\{\Delta F = \Delta U - T\Delta S\}$. The delay rates $e^{-\Delta F/T}$ will be from energy barriers ($\sim e^{-\Delta U/T}$) and entropy barriers ($\sim e^{-|\Delta S|}$), schematically depicted in Fig 1. Ritort and colleagues⁶⁻⁹ have proposed a Partial Equilibration Scenario (PES) for re-equilibrations delayed by *entropy* barriers. Over a waiting time t_w , a post-quench ageing system rapidly explores configuration shells of energy $E(t_w)$, entropy $S(E)$, and (inverse) micro-canonical effective temperature $1/T_{eff}(t_w) \equiv dS(E)/dE$. Passages to a lower shell of $E(t_w + 1) \equiv E' = E(t_w) + \delta E$ are driven by spontaneous heat releases ($\delta E = \delta Q < 0$) to the bath at T . The PES says that an iteration of these cooling steps ratchets the system down to the new canonical equilibrium. The non-equilibrium probability distribution for energy changes^{6,8} $P_0(\delta E; t_w)$ is peaked at positive energies, with an exponential tail for $\delta E < 0$, whose fall-off $\sim e^{\delta E/2T_{eff}(t_w)}$ determines the effective temperature. The PES distribution has been studied by *analytic* Monte Carlo (MC) methods for harmonic oscillators⁸, and by numerical MC simulations of spin glasses and Lennard-Jones liquids^{7,9}. We note that if the effective temperature of the heat-release probability vanishes at some $T = T_d$, then there is an arrest of the PES cooling process.

We consider solid-solid structural transitions of martensites¹⁰⁻¹⁶, quenched below a thermodynamic T_0 , with competing domains and slow relaxations^{11,17}. Martensites undergo first-order, diffusionless transitions^{5,10} from the higher-symmetry austenite, with atomic shifts locked to their unit-cell

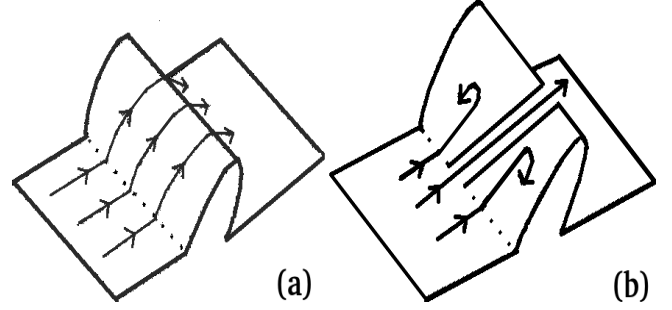


FIG. 1. Schematic of delays from two limits of free energy barriers: a) Energy-barrier delays from thermally activated jump attempts. b) Entropy-barrier delays from searches for rare passages. Key seeks lock, most attempts fail.

distortions ('military transformations'). The order-parameter strains have degenerate lower-symmetry 'variants' separated by crystallographically oriented Domain Walls (DW), that can form complex microstructures^{10,14,15}. A long-standing puzzle^{11,12} is that while quenches of austenite to below an (athermal) 'martensite start' temperature $T_1 > T$ results in avalanche martensitic conversions, quenches above it $T_1 < T$, show *delayed conversions* instead of no conversions. Resistivity, as a transition diagnostic, is flat during post-quench 'incubations', that end in sudden drops at a delayed avalanche¹¹. Delays rise sharply, for shallower quenches approaching a third temperature T_d that is in between, $T_1 < T_d < T_0$. When a bath quench T goes a few percent closer to T_d , the resistivity-drops go from a few seconds after, to ten thousand seconds after, the temperature quench¹².

In this Letter we do MC simulations in *three* dimensions, with vector order parameter strains, for four structural transitions¹⁸. We present here the cubic-tetragonal (CT) transition¹⁵, with a strain order parameter of components $N_{OP} = 2$, with three competing unit-cell 'variants' $N_V = 3$. We confirm for all four transitions, that the PES energy change distribution has the predicted generic behaviour: an exponential tail, with an effective

temperature that regulates heat releases⁶⁻⁹.

For our specific case of quenches across a first order transition, the Order Parameter (OP) rises from zero, enabling the waiting time t_w to be defined by rising-OP marker events at t_m , that depend on T . This choice $t_w = t_m(T)$ induces quench-temperature dependences: $T_{eff}(t_w) \rightarrow T_{eff}(T)$ and $P_0(\delta E; t_w) \rightarrow P_0(\delta E, T)$. For passages to lower energy shells, the OP evolution must satisfy T -controlled entropy-barrier constraints, postulated as of two types: a) A constraint that OP configurations must find and enter a Fourier space bottleneck that is like a Golf Hole (GH) that funnels into fast passage, as suggested for protein folding¹⁹; or b) A constraint that the OP states need transient catalysts to enable fast passages, as inspired by facilitation models²⁰⁻²². Our case is a), and we find a linear vanishing $T_{eff}(T) \sim (T_d - T)$. The ‘search freezing’ temperature T_d occurs at a pinch-off on warming, of the \vec{k} -space inner radius of an angularly modulated bottleneck. Equilibration times are exponential in entropy barriers^{11,12,23}, and for quenches $T_d > T > T_1$, diverge as $\bar{t}_m(T) \sim e^{1/T_{eff}(T)} \sim e^{1/(T_d - T)}$. Thus VFT-like behaviour is not restricted to the glass transition. Conversely, entropy barriers vanish and delay times collapse for $T < T_1$, when the bottleneck expands to span the Brillouin zone.

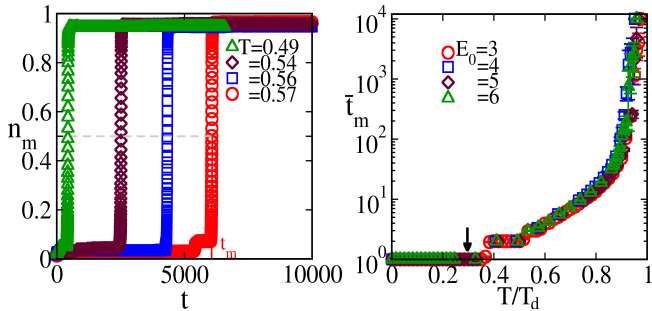


FIG. 2. *Delay times for CT martensitic conversion:* The martensite fraction $n_m(t_m) = 0.5$ defines t_m . a) For $T \leq T_1$ avalanche conversions occur, at $t_m = 1$. For $T_d > T > T_1$ DW sluggishness causes ‘incubation’ delays or postponement of conversion avalanches to $t = t_m(T)$. b) Log-linear plot of mean delay time $\bar{t}_m(T)$ versus $T/T_d < 1$. Delay times are not exponentially sensitive to Hamiltonian energy scales E_0 , so are not activated: delays are from *entropy* barriers.

We derive a discretized-strain Hamiltonian¹⁵ in 3D, from a crystal-symmetry invariant strain free energy F , that has Compatibility¹⁴, Ginzburg, and Landau terms in $F/E_0 = \sum_{\vec{r}, \vec{r}'} f_C + \sum_{\vec{r}} [f_G + f_L]$, with E_0 an energy scale. There are six independent *physical* strains¹⁵ in 3D, that are linear combinations of Cartesian tensor strains: compressional e_1 ; deviatoric or rectangular e_2, e_3 , and shear e_4, e_5, e_6 . The OP of the cubic-tetragonal (CT) transition are two deviatoric strains $\vec{e} = (e_3, e_2) = (\frac{1}{\sqrt{6}}\{e_{xx} + e_{yy} - 2e_{zz}\}, \frac{1}{\sqrt{2}}\{e_{xx} - e_{yy}\})$. Austenite is $\vec{e} = \vec{0}$.

The remaining $6 - N_{OP}$ non-OP strains (one com-

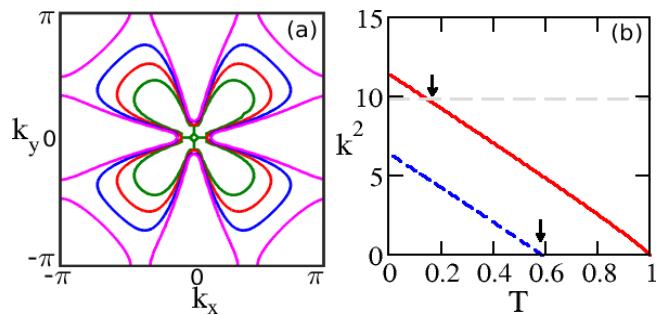


FIG. 3. *Bottlenecks in Fourier space for CT transition:* The temperature dependence of bottleneck size and shape is shown for a $[1,1,1]$ slice of a 3D anisotropic bottleneck. a) The 2D slice in (k_x, k_y) is like an anisotropic ‘Golf Hole’, enclosing negative martensite states, that shrinks with warming T . The open butterfly shape changes topology to a segmented four-petal flower shape at $T = T_d$. b) The anisotropic bottleneck inner and outer radii k_{in}, k_{out} are plotted as k^2 vs T . The bottleneck outer radius $k_{out}(T)$ for $0 < T \leq T_1$ (arrow) spans a Brillouin Zone size of $\sim \pi$ (horizontal light dashes), so conversions are immediate. The outer radius shrinks to a point on the right at the thermodynamic transition $T = T_0 = 1$ to austenite-only states. On the other hand, the inner radius $k_{in}(T)$ shrinks on warming for $0 \leq T \leq T_d$, vanishing (arrow) at $T = T_d$ when the outer radius is still nonzero: the bottleneck topology changes.

pressional and three shears) enter the Hamiltonian as harmonic springs. These are minimized subject to a linear St Venant Compatibility constraint¹⁴ that says no dislocations are generated: the double-curl of the strain tensor must vanish. There are three independent algebraic equations in \vec{k} space, connecting OP and non-OP strains¹⁵. The harmonic non-OP strains then analytically yield an OP-OP interaction, whose transition-specific, *anisotropic* Compatibility kernel¹⁵ is a 2×2 matrix, $U_{\ell\ell'}(\hat{k})$ where $\ell, \ell' = 2, 3$. There is a prefactor of $(1 - \delta_{\vec{k}, \vec{0}})$, and dependence on direction $\hat{k} = \vec{k}/|\vec{k}|$.

The Landau free energy for CT is $f_L(\vec{e}) = [(\tau - 1)\vec{e}^2 - 2(e_3^3 - 3e_3e_2^2) + \vec{e}^4]$ and has 4 minima, at $N_V = 3$ variants plus at zero strain. Here $\tau(T) \equiv (T - T_c)/(T_0 - T_c)$, and $\tau(T_c) = 0$ at the spinodal T_c , while $\tau(T_0) = 1$ at the first-order transition temperature, scaled to be unity $T_0 = 1$.

In ‘polar’ coordinates, $\vec{e} \equiv |\vec{e}|\vec{S}$. Here the unit-magnitude ‘variant vectors’ $\vec{S}(\vec{r})$ specify the unit-cell variants on either side of a Domain Wall (DW), that can be martensite-martensite or martensite-austenite. The nonzero $N_V = 3$ martensite-variants have spins¹⁵ $\vec{S} = (S_3, S_2) = (1, 0), (-1/2, \sqrt{3}/2), (-1/2, -\sqrt{3}/2)$, pointing to corners of an equilateral triangle in a unit circle, while the centroid $\vec{S} = (0, 0)$ is austenite. Thus $\vec{S}^2 = 0$ or 1 .

The degenerate Landau minima are at mean-OP magnitudes $\bar{\varepsilon}(T) = (3/4)[1 + \sqrt{1 - (8\tau/9)}]$. The variant domains have mostly-flat strain magnitudes, approximated by $\bar{\varepsilon}(T)$. Substituting $\vec{e}(\vec{r}) \rightarrow \bar{\varepsilon}(T)\vec{S}(\vec{r})$, the Landau term becomes $f_L(\vec{e}) \rightarrow f_L(T)\vec{S}(\vec{r})^2$. Here $f_L(T) \equiv$

$\bar{\varepsilon}(T)^2 g_L(T) \leq 0$, where $g_L = (\tau - 1) + (\bar{\varepsilon}(T) - 1)^2 \leq 0$. At $T = T_0^-$, the OP is unity $\bar{\varepsilon} = 1$ and $g_L = 0$.

Notice a separation of time scale responses to T quenches: the OP magnitude $\bar{\varepsilon}(T)$ responds immediately, at $t = 1$, while Domain Walls can take thousands of time steps t , to evolve successively from DW Vapour to DW Liquid to a DW Crystal of twins. For our case of shallow quenches $T_d > T > T_1$, it is the DW Vapour-to-Liquid conversion has the long (bottleneck type) delays studied here. See Videos²¹ A,B. The DW moves by correlated flips of spins that bracket it, while domain spins remain locked: a dynamical heterogeneity in space and time^{3,5}. [For deeper quenches $T \ll T_1$ not studied here, it is the DW Liquid-to-Crystal twin orientation that has long (facilitation type) delays. See Video²¹ C.]

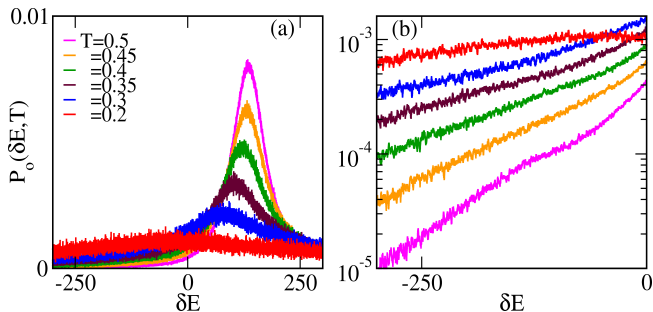


FIG. 4. *Energy-change statistics for CT transition:* a) Linear-linear plot of the normalized probability $P_0(\delta E, T)$ versus energy change δE , for six T quenches. b) Log-linear version. Slope at the origin $\beta_{eff}(T)/2$ rises from zero for $T > T_1$.

The total hamiltonian is $\beta H = \beta H_L + \beta H_G + \beta H_C$, without extrinsic disorder. It is diagonal in Fourier space,

$$\beta H = \frac{D_0}{2} [\sum_{\ell, \ell'} \sum_{\vec{k}} [\epsilon_{\ell, \ell'}(\vec{k}, T) \vec{S}_{\ell}(\vec{k}) \vec{S}_{\ell'}^*(\vec{k})]], \quad (1)$$

with $D_0 \equiv 2\bar{\varepsilon}(T)^2 E_0/T$. The spectrum, with $K_{\mu}(\vec{k}) \equiv 2 \sin(k_{\mu}/2)$ and $\mu = x, y, z$, is

$$\epsilon_{\ell, \ell'}(\vec{k}, T) \equiv \{g_L(T) + \xi_0^2 \vec{K}^2\} \delta_{\ell, \ell'} + \frac{A_1}{2} U_{\ell, \ell'}(\hat{k}). \quad (2)$$

The anisotropic Compatibility kernel in the energy spectrum can induce preferred DW orientations^{14-16,21}. For example the $\ell = \ell'$ kernel $U_{\ell, \ell}(\hat{k})$ is smallest $U_{\ell, \ell}(min) = 0$ at the most favoured orientation, and largest $U_{\ell, \ell}(max) > 0$ for most disfavoured. The negative sign of the Landau term $H_L \sim g_L < 0$ and the positive signs of the Ginzburg term $H_G \sim \vec{k}^2 > 0$ and the Compatibility term $H_C > 0$ imply the spectrum $\epsilon_{\ell, \ell}(\vec{k}, T)$ could vanish along some Fourier contour. This contour will be angularly modulated, through the anisotropy of the Compatibility kernel^{15,16}.

In MC simulations, the initial state $t = 0$ is high-temperature austenite that is randomly and dilutely (2%) seeded with martensite unit-cells. Typical parameters are $T_0 = 1$; $\xi_0^2 = 1$; $T_c = 0.95$; $E_0 = 3$; system

volume $N = L^3 = 16^3$; $N_{runs} = 100$; and holding times $t_h = 10^4$ MC sweeps. The martensite fraction is $n_m(t) \equiv \frac{1}{N} \sum_{\vec{r}} S^2(\vec{r}, t) \leq 1$, with $n_m = 0$ or 1 for uniform austenite or martensite. The conversion time t_m is defined as when¹⁶ $n_m(t_m) = 1/2$. An athermal martensite droplet or embryo can rapidly form anywhere, and after waiting till $t_w = t_m$, can *propagate* rapidly to the rest of the system¹³. Hence it is mean *rates* \bar{r}_m (or inverse times), that are averaged over runs, analogous to total resistors in parallel determined by the smallest resistance. Mean times \bar{t}_m are inverse mean rates: $\bar{t}_m(T) \equiv 1/\bar{r}_m(T)$.

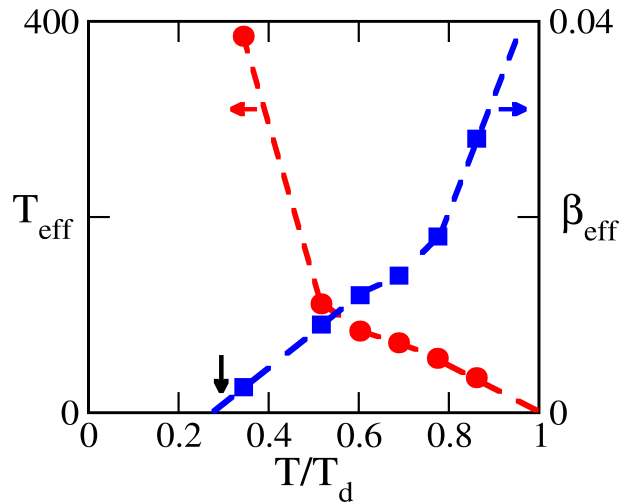


FIG. 5. *Effective temperature and its inverse, versus quench temperatures for CT transition:* Left vertical axis: $T_{eff}(T)$ versus T/T_d appears to vanish as $\sim (T_d - T)$, and rises from $T_1 < T_d$. Right vertical axis: $\beta_{eff}(T)$ appears to vanish as $\sim (T - T_1)$, and rises rapidly towards $T_d > T_1$. The entropy barrier $S_B \sim \beta_{eff}$ will then vanish at T_1 (downward arrow) or diverge at T_d . Dashed lines are guides to the eye.

The MC procedure is standard, but with a crucial extra data retention⁶⁻⁹ of energy changes.

0. Take N sites, each with a vector spin of N_{OP} components, in one of $N_V + 1$ possible values (including zero) at MC time t . Each $\{\vec{S}(\vec{r})\}$ set is a ‘configuration’.

1. Randomly pick one of N sites, and randomly flip the spin on it to a *new* direction/value, and find the (positive/negative) δE changes for the new configuration.

2. If the energy change $\delta E \leq 0$, then accept the flip. If $\delta E > 0$, then accept flip with probability $e^{-\delta E/T}$. Record this δE , that is not usually retained after use.

3. Repeat steps 1 and 2. Stop after N such spin-flips. This configuration has the conversion fraction $n_m(t + 1)$.

4. We collect²⁴ all $\{\delta E\}$ from each spin-flip (configuration change) within each MC sweep of every run, up to the conversion time for that run, $t \leq t_m(T) \leq t_h$. The set size $N \times t_m \times N_{run}$ has up to $16^3 \times 10^4 \times 100$ data points. We take six quenches, from $T = T_1$ up to T_d .

Figure 2a shows $n_m(t)$, the martensite conversion-fraction in a *single* run, versus MC time t for different temperatures T . For quenches $T \leq T_1$, avalanche con-

versions, characteristic of athermal martensite, occur in the very first sweep over all spins ($t = 1$). We identify T_1 with the martensite start temperature^{11,12} $M_s = T_1$. For higher temperatures $T > T_1$, there is a curious ‘incubation’ period, when nothing happens macroscopically, until a postponed avalanche at $t_w = t_m$. These models^{16,24} display the delayed transitions and burst-like growth of order, characteristic of martensites and manganites^{11,12,17}. Fig 2b shows that for T above T_1 (downward arrow), and approaching T_d , the mean incubation delays rise steeply, due to entropic bottlenecks.

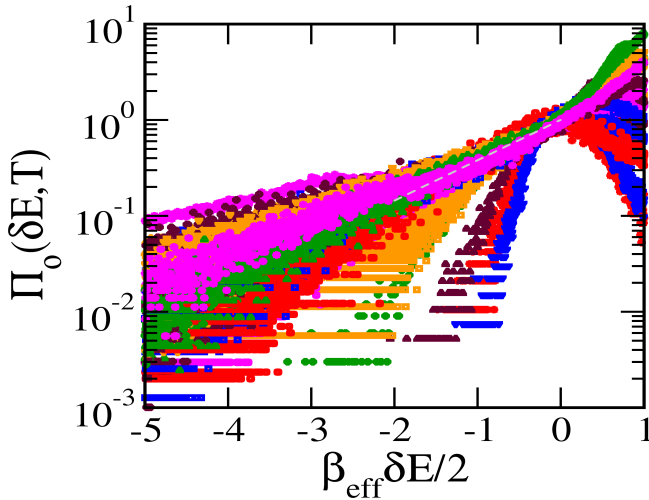


FIG. 6. *Universal slope of PES distribution:* Log-linear scaled plot of $\Pi_0(\delta E, T) \equiv P_0(\delta E, T)/P_0(0, T)$ versus $z \equiv \beta_{eff}(T)\delta E/2$. The PES predicts a universal slope of unity at $z = 0$. The four transitions mentioned have respective slope averages and standard deviations of 1.000 ± 0.045 , 1.025 ± 0.036 , 1.009 ± 0.08 , 0.850 ± 0.085 . The data for six T and four transitions have mean slope (dashed white line) of 0.97 ± 0.06 .

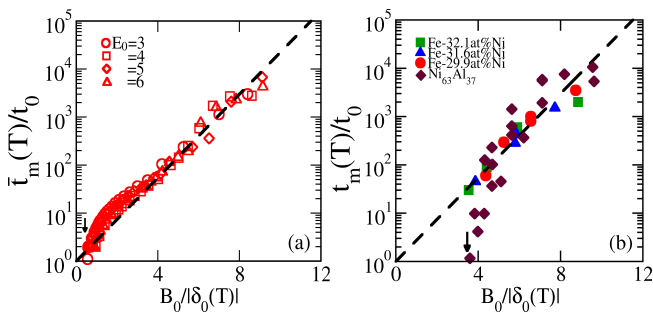


FIG. 7. *Log-linear plots of scaled time versus (inverse) scaled temperature deviation:* Scaled conversion times t_m/t_0 versus $B_0/|\delta_0|$ with parameters t_0, B_0 extracted from data. There is Vogel Fulcher linearity near T_d , with falloffs near T_1 (downward arrows). a) From CT simulations in 3D for different E_0 . b) From experiments^{11,12} in 3D for different alloys.

For our model, the boundary of a 3D bottleneck is from the spectrum set equal to zero $\epsilon_{\ell, \ell}(\vec{k}) = 0$, defin-

ing an *anisotropic* surface in \vec{k} -space. For the CT case, a $[1,1,1]$ slice can intersect the bottleneck surface as an open, butterfly-shaped locus with an inner and outer radius, inside the Brillouin Zone (BZ). See Fig 3. For $T \leq T_1$, the radius $k_{out}(T)$ is larger than a BZ scale $\sim \pi$, and martensitic passages are immediate. For $T_1 < T < T_d < T_0$, the butterfly bottleneck shrinks on warming. At $T = T_d$, the inner squared-radius $k_{in}(T)^2 = |g_L(T)| - (A_1/2)U_{\ell, \ell}(max)$ vanishes, and the topology of the connected butterfly changes to that of a segmented four-petaled flower: entropy barriers diverge, and PES heat releases are arrested. For the ‘precursor’ region¹⁴ $T_d < T < T_0$, PES passages are energetically available, but entropically inaccessible. Repeated bottleneck entry attempts could induce vibrations. See Video²¹ D. Finally, at $T = T_0 = 1$, the outer squared-radius $k_{out}(T)^2 = |g_L(T)|$ also vanishes: the bottleneck becomes a point, and only austenite exists.

We collect the $O(1)$ changes $\{\delta E\}$ to the $O(N)$ energy E . The probability $P_0(\delta E, T)$ to access E' from E , is proportional to the number of target states $\Omega(E')$. With $S(E') = \ln \Omega(E')$, the probability ratio $R_0(\delta E)$ of energy changes is related to the entropy change $\Delta S(\delta E) \equiv S(E') - S(E) < 0$ by a fluctuation relation for aging¹⁻⁴:

$$R_0 \equiv \frac{P_0(\delta E, T)}{P_0(-\delta E, T)} = \frac{\Omega(E')}{\Omega(E)} = e^{\Delta S(\delta E)}. \quad (3)$$

Entropy barriers $S_B \equiv -\Delta S > 0$ rise, when the searched-for states become rarer. Since $R_0(\delta E)R_0(-\delta E) \equiv 1$, the entropy change is odd, $\Delta S(\delta E) + \Delta S(-\delta E) = 0$, and a solution for the PES distribution is

$$P_0(\delta E, T) = P_0^{(+)}(\delta E) e^{\frac{1}{2}\Delta S(\delta E)}, \quad (4)$$

with an even $P_0^{(+)}(\delta E) \equiv \sqrt{P_0(\delta E, T) P_0(-\delta E, T)}$. The leading entropy-change term for small heat releases is $\Delta S \simeq \beta_{eff} \delta E$ where $\beta_{eff} \equiv 1/T_{eff}$. For $\delta E = -|\delta E| < 0$, the Boltzmann-like form $P_0 \simeq e^{-\frac{1}{2}\beta_{eff}(T)|\delta E|}$ gives a physical meaning to the effective temperature, as a *search range* denoting accessible energy shells. If $\beta_{eff} \rightarrow 0$, entropy barriers collapse, and passages are immediate. If $T_{eff} \rightarrow 0$, then entropy barriers diverge, and passages cease. Glass-like freezing is a shutdown of PES searches.

Fig 4a shows that, as in PES models⁶⁻⁹, the $P_0(\delta E, T)$ peaks are at positive δE , understood as a completion-of-square between a gaussian peaked at the origin and an exponential tail for $\delta E < 0$. Fig 4b shows a zoom-in near the origin, where the slopes define $\frac{1}{2}\beta_{eff}(T)$.

Fig 5 shows the dependence of $\beta_{eff}(T)$ and $T_{eff}(T)$ on the quench temperature T . The data suggest a linear vanishing of $T_{eff} \simeq (T_d - T)/(B_0 T_d)$ near T_d , at a search freezing and a suppression of the heat releases to the bath. There is also a linear vanishing of $\beta_{eff} \sim T - T_1$ near T_1 , at a search avalanche and prompt equilibration.

Fig 6 shows log-linear plots for a scaled $\Pi_0(\delta E, T) \equiv P_0(\delta E, T)/P_0(0, T)$ versus the entropy-barrier related

variable $\frac{1}{2}\beta_{eff}\delta E$. Data are for four 3D structural transitions^{18,23}, and six T between the collapse (T_1) and divergence (T_d) of entropy barriers.

The mean conversion time is exponential in the entropy barrier²³ $\bar{t} \sim e^{1/T_{eff}(T)}$, so near T_d we have $\bar{t}_m(T) \simeq t_0 e^{B_0/|\delta_0(T)|}$, where the constants B_0, t_0 can be fixed by simulational and experimental data²⁴. The initial slope in $|\delta_0|$ of $1/\ln \bar{t}_m(T)$ gives $1/B_0$; and the extrapolated intercept of $\ln \bar{t}_m(T)$ versus $B_0/|\delta_0(T_0)|$ gives t_0 . For Ni-Al data¹¹ the ‘fragility’ parameter² $B_0 T_d \simeq 1.23$ Kelvin, and the austenite-martensite DW hop time is $t_0 \simeq 1$ sec.

Fig 7a shows that CT times show VFT behaviour near T_d and fall-off behaviour near T_1 . Fig 7b shows data extracted from Ni-Al and Fe-Al alloys^{11,12} are similar.

Signatures of PES could be sought, in previous simulations or experiments^{3,5} under systematic temperature quenches, with a recording of energy releases. Further

experimental work on martensitic alloys^{11,12} could record signal and noise under systematic quench steps of $1/|\delta_0|$, over the delay region $T_d > T > T_1$; as well as the precursor^{14,21} region $T_0 > T > T_d$ above it. Non-stationary distributions of energy releases might be determined through concurrent resistive, photonic, acoustic, and elastic signals²⁵. Finally, one might speculate that complex oxides quenched near their structural/functional transitions, could show PES ageing behaviour in their (strain-coupled) functional variables^{17,18}.

In summary, post-quench ageing in athermal martensites shows characteristic signatures of the Partial Equilibration Scenario. The conversion arrest and delay-divergence found in 3D simulations and alloy experiments, are understood as arising from a vanishing of the search temperature that governs the PES cooling process.

Acknowledgement: It is a pleasure to thank Smarajit Karmakar for valuable discussions on the glass transition.

-
- ¹ K. Binder and W. Kob, *Glassy Materials and Disordered Solids*, World Scientific, Singapore (2005).
- ² A.L. Greer, K.F. Kelton, S. Sastry, Eds., *Fragility of glass-forming liquids*, Hindustan Book Agency, New Delhi (2014).
- ³ P. Harrowell, Nature Phys **2**, 157 (2006); H. Shintani and H. Tanaka, Nature Phys **2**, 200 (2006); X. Yang, H. Tong, W-H. Wang, and K. Chen, Phys. Rev. E, **99**, 062610 (2019).
- ⁴ P. Lunkenheimer, S. Kastner, M. Koehler and A. Loidl, Phys. Rev. E **81**, 051504 (2010).
- ⁵ H. Fang, M.F. Hagan, W.B. Rogers, Proc. Nat. Acad. Sci., **117**, 27927 (2020).
- ⁶ F. Ritort, J.Phys. Chem B **108**, 6893 (2004); and in *Unifying Concepts in Granular Media and Glasses*, (eds.) A. Coniglio, A. Fierro, H.J. Hermann and M. Nicodemi, Elsevier (2004); arXiv/ condmat/ 0311371v1.
- ⁷ A. Crisanti and F. Ritort, Europhys. Lett., **66**,253 (2004).
- ⁸ L. L. Bonilla, F.G. Padilla and F. Ritort, Physica A **250**, 315 (1998); L. Garriga and F. Ritort, Phys. Rev. E **72**, 031505 (2005).
- ⁹ A. Crisanti, M. Pecco and F. Ritort, Phys. Rev. Lett., **110**, 080601 (2013).
- ¹⁰ K. Bhattacharya, *Microstructure of Martensite*, Oxford University Press (2003).
- ¹¹ T. Kakeshita, T. Fukuda and T. Saburi, Scripta Mat. **34**, 1 (1996); T. Kakeshita, K. Kuroiwa, K. Shimuzu, T. Ikeda, A. Yamagashi, and M. Date, Mat. Trans. JIM, **34**, 423 (1993).
- ¹² M. Aspelmeier, U Klemradt, L.T. Wood and S.C. Moss, Phys. Stat. Sol. (a) **174**, R9 (1999); L. Müller , U. Klemradt, T.R. Finlayson, Mat. Sci. and Eng. A **438**, 122 (2006); L. Müller, M. Waldorf, G. Gutt, G. Grubel, A. Madsen, T. R. Finlayson and U. Klemradt, Phys. Rev. Lett., **109**,105701 (2011).
- ¹³ P.R. Rios and J.R.C. Guimaraes, Scripta Mat., **57**, 1105 (2007); P.R. Rios, F.G. Cardoso, T.A. Neves and J.R.C. Guimaraes, in the Minerals, Metals and Materials Society, TMS 2015 144th Annual Meeting, Cham, Springer (2015), https://doi.org/10.1007/978-3-319-48127-2_84.
- ¹⁴ S. Kartha, J. A. Krumhansl, J. P. Sethna, and L. K. Wickham, Phys. Rev. **B** 52, 803 (1995).
- ¹⁵ S.R. Shenoy, T. Lookman and A. Saxena, Phys. Rev. B **82**, 144103 (2010). The kernels for the four 3D transitions are in an Appendix. K.O. Rasmussen, T. Lookman, A. Saxena, A.R. Bishop, R.C. Albers and S.R. Shenoy, Phys. Rev. Lett., **87**, 055704 (2001).
- ¹⁶ N. Shankaraiah, K. P. N. Murthy, T. Lookman and S. R. Shenoy, Europhys. Lett. **92**, 36002 (2010); Phys. Rev. B **84**, 064119 (2011); Phys. Rev. B **91**, 214108 (2015).
- ¹⁷ W.I.F. David, C.C. Wilson, P. P. Edwards, R. Jones, M.R. Harrison, Nature **331**, 245 (1988); M. Uehara and S-W. Cheong, Europhys. Lett., **52**, 674 (2000); V Podzorov, C.H. Chen, M.E. Gershenson and S.-W. Cheong, Europhys. Lett., **55**, 411 (2001); V. Podzorov, B.G. Kim, V. Kiryukin, M.E. Gershenson and S.W. Cheong, Phys. Rev. B **64**, 140406 (R) (2001); V. Hardy, A. Maignan, S. Hebert, C. Yaicle, C. Martin, M. Hervieu, M.R. Lees, G. Rowlands, D. McK. Paul and B. Raveau, Phys. Rev. B **68**, R220402 (2003); V. Hardy, S. Majumdar, S.J. Crowe, M.R. Lee, D. McK. Paul, L. Herve', A. Maignan, S. Hebert, C. Martin, C. Yaicle, M. Hervieu and B. Raveau, Phys. Rev. B **9**, 020407 (R) (2004).
- ¹⁸ The four chosen structural transitions can occur in materials with useful functionalities¹⁷. The transitions are: tetragonal-orthorhombic (*YBCO*, superconductivity); cubic-tetragonal (*FePd*, shape memory); cubic-orthorhombic (*BaTiO*, ferroelectrics); cubic-trigonal (*LaSrMnO*, colossal magnetoresistance).
- ¹⁹ D. J. Bicout and A. Szabo, Protein Science **9**, 452 (2000); P.G. Wolynes, Proc. Amer. Phil. Soc. **145**, 4 (2001); M. Cieplak and J.I. Sulkowska, J. Chem. Phys., **123**,194908

(2005).

- ²⁰ F. Ritort and P. Sollich, Adv. Phys. **52**, 219 (2003);
K. Otsuka, X. Ren, and T. Takeda, Scripta Mat. **45**,145 (2001).

- ²¹ Supplementary Material. [URL]

Videos for the 2D square-rectangle $N_{OP} = 1, N_V = 2$ transitions for 64×64 systems, with austenite (green) and the two martensite variants (red/ blue), show¹⁶ sequentially evolving Domain Wall states, from DW Vapour to DW Liquid to DW Crystal or oriented ‘twins’. The 3D physical evolutions are similar.

Video A. The droplet in \vec{r} -space: This shows the coordinate-space evolution for $T_d > T > T_1$, for the bottleneck type passage. Random initial martensite seeds rapidly form a single-variant DW Vapour droplet, bounded by a martensite-austenite DW. This fluctuates like an amoeba, searching over incubation delays for a conversion passage to a DW Liquid, and then a quick symmetry-breaking to a DW crystal.

Video B. The droplet in \vec{k} -space: This shows the $T_d > T > T_1$ evolution as Video A but now in Fourier space. The dynamic structure factor for variant spins $|S(\vec{k}, t)|^2$ is shown in (k_x, k_y) space, with elliptic contours of a DW Vapour going to the bi-diagonal X of a DW Liquid, and to a single-diagonal $k_y = -k_x$ line of a DW Crystal.

Video C. The \vec{r} -space dynamic catalysts: This shows the evolution for deep quenches to $T \ll T_1$, of the facilitation type passage²⁰. The DW Vapour now converts rapidly to a sluggish DW Liquid of frozen walls. Transient hotspots of austenite in martensite act as facilitation variables or dynamic catalysts, that unlock and delete even far-off minority-diagonal DW segments, leaving a dominant-diagonal DW crystal, or twins¹⁶.

Video D. The \vec{r} -space tweed precursor: This shows (dy-

namical) tweed¹⁴ in the precursor region $T > T_d > T_1$, of an oscillating array of martensitic islands in austenite sea. This might arise from a \vec{k} space profile of the droplet, vibrating as it unsuccessfully attempts entry to a topologically blocked GH.

- ²² S. R. Shenoy and T. Lookman, Phys. Rev. B **78**, 144103 (2008), see Fig 7.

- ²³ The mean equilibration rate is the average over an inter-shell rate $1/t(\delta E)$ over all heat releases. With a normalized PES probability, $1/\bar{t} = \int_{-\infty}^0 d\delta E P_0(\delta E, T)/t(\delta E)$. For slow intershell variation $1/t(\delta E) \simeq 1/t_0$, the mean rate is proportional to the acceptance fraction over energy decrements. Taking the PES probability, as a shifted gaussian with peak mean energy change $M > 0$, and variance $\sigma^2 = 2MT_{eff}$, the acceptance fraction is a complementary error function, whose asymptotic behaviour yields $t_0/\bar{t} \simeq e^{-M/4T_{eff}}$. Dropping constants, the martensitic mean conversion time near T_d is written simply as $\bar{t}_m(T) = t_0 e^{1/T_{eff}(T)}$.

- ²⁴ N. Shankaraiah, K.P.N. Murthy and S.R. Shenoy, submitted.

- ²⁵ U. Chandni, S Kar-Narayan, A. Ghosh, H.S. Vijaya and S. Mohan, Acta Mater., **57**,6113 (2009);
A. Planes, Ll. Manosa and E. Vives, J. Alloys and Comp., **577**, S699 (2013);
X. Balandraud, N. Barrara, P. Biscarin, M. Grediac, G. Zanzotto, Phys. Rev. B, **91**,174111 (2015);
B. Blaysat, X. Balandraud, M. Grediac, E. Vives, N. Barrera and G. Zanzotto, Nature Commun. Mater., **1**,3 (2020);
Z. Eranson, B. Ruta, S. Hechler, M. Stolpe, E. Pineda, I. Gallimo, and R. Busch, Phys. Rev. Lett., **115**, 175701 (2015).See also Physics **8**, S5121 (2015).